Soft Matter

Accepted Manuscript

ROYAL SOCIETY OF CHEMISTRY

www.rsc.org/softmatter

Journal Name

ARTICLE

Switchable 3D liquid crystal grating generated by periodic photo-alignment on both substrates

Received 00th January 20xx,
Accepted 00th January 20xx

DOI: 10.1039/x0xx00000x

www.rsc.org/

I. Nys,[ab] J. Beeckman[ab] and K. Neyts[ab]

A planar liquid crystal (LC) cell is developed in which two photo-alignment layers have been illuminated with respectively a horizontal and a vertical diffraction pattern of interfering left- and right-handed circularly polarized light. In the bulk of the cell, a complex LC configuration is obtained with periodicity in two dimensions. Remarkably, the period of the structure is larger than the period of the interference pattern, indicating that lowering of the symmetry allows a reduction in the elastic energy. The liquid crystal configuration depends on the periodicity of the alignment but also on the thickness of the cell. By applying a voltage over the electrodes, the power going into the different diffracted orders can be tuned. Finite element (FE) simulations based on Q-tensor theory are used to find the 3D equilibrium director distribution, which is used to simulate the near-field transmission profile based on the Jones calculus. A 2D Fourier transform is performed for both the *x*- and *y*-component of the transmitted wave to find the diffraction efficiency.

Introduction

Liquid crystals (LCs) are widely used in display applications and their unique electro-optic properties also make them suitable for the use in photonic components such as optical filters, switches, beam-steering devices, spatial light modulators, lasers, and optical nonlinear components[1-8]. Multiple techniques such as mechanical rubbing, ion beam etching and oblique deposition of inorganic material have been investigated in the past to control the LC alignment near the surface. Photo-alignment materials recently gained popularity thanks to the flexibility to align liquid crystals in complex configurations that cannot be obtained with common alignment techniques. They offer interesting possibilities if geometrical constraints make mechanical rubbing problematic and if high-resolution LC configurations with micrometer or submicrometer resolution are envisioned[9-12]. With the help of photo-alignment material, a good alignment can be obtained on curved surfaces, thin capillaries and multi-domain pixels. In recent years, photo-alignment materials have been extensively used to align LCs in optical polarization gratings[13-20]. The cell is illuminated with an interference pattern of right- and left-handed circularly polarized light (figure 2). This results in a continuously rotating alignment on both substrates that can be represented by a director field that is independent of the z-coordinate: $\boldsymbol{n}(x,y,z) = \sin\left(\frac{\pi x}{\Lambda}\right)\mathbf{1}_x + \cos\left(\frac{\pi x}{\Lambda}\right)\mathbf{1}_y$ (figure 1). Note that the director is represented by a vector, but there is no physical difference between ***n*** and ***-n***. These liquid crystal polarization gratings can be switched with modest drive voltages and can have a high diffraction efficiency[16].

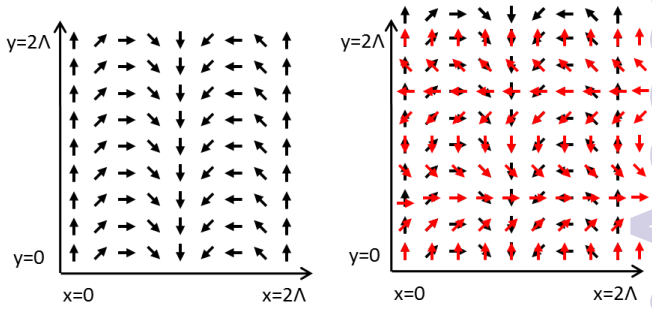

Figure 1 1D (left) and 2D (right) LC polarization grating

In this work, we use the same interference pattern of right- and left-handed circularly polarized light to illuminate both photo-alignment coated substrates but, before the cell is assembled, one of the substrates is rotated over 90°. As a result, the alignment direction on the bottom substrate varies along the *x*-direction and on the top substrate it varies along the *y*-direction (figure 1). This gives rise to a three-dimensional LC configuration in the bulk and a two-dimensional diffraction pattern. The LC configuration depends on the periodicity Λ and the thickness *d* of the cell. By applying a voltage over the liquid crystal layer, the diffraction pattern can be tuned. Other techniques for the formation of three-dimensional LC vector holograms and twisted nematic LC gratings with interesting diffraction properties have been reported earlier by Sasaki et al.[21] and Choi et al.[22]

[a] Liquid Crystals & Photonics Group, Department of Electronics and Information Systems, Ghent University, Sint-Pietersnieuwstraat 41, B-9000 Ghent, Belgium
[b] Center for Nano- and Bio- photonics, Ghent University, Sint-Pietersnieuwstraat 41, B-9000 Ghent, Belgium

In the following sections we discuss the experimental details of the used setup and analyze the polarized microscope images of the LC grating. Finite element simulations based on Q-tensor theory are performed to find the 3D equilibrium director distribution and this result is used to simulate the near-field transmission profile based on the Jones calculus. The simulated results for the transmission are compared to the experimental results. Finally the far-field diffraction characteristics are analyzed as a function of the applied voltage both experimentally, theoretically and by simulations.

Experimental setup

For the experiments, the nematic liquid crystal E7 is used. The cell consists of two parallel glass substrates, each covered with an indium tin oxide (ITO) electrode and a photo-alignment layer. Both PAAD22 (Beamco) and sulfonic azo dye SD1 have been used as alignment layer and give comparable results[23]. The photo-alignment layer is spin-coated on the glass substrates (3000rpm, 30s) and illuminated with an interference pattern of right- and left-handed circularly polarized UV light beams making an angle θ_{UV} of 1.56° with the substrate normal (figure 2). We use a continuous wave single-mode UV laser emitting at 355nm (Coherent, Genesis CX SLM, 100mW). The interference pattern has a periodicity $\Lambda = \lambda_{UV}/2\sin(\theta_{UV})$ of 6.5µm and the director vector exhibits a periodicity of $2*\Lambda$=13µm as shown in Fig. 1. The power in each beam is 30mW and the sample is illuminated during 90s. The spot size is approximately 1cm². Both glass substrates are illuminated with the same interference pattern but they are rotated over 90° compared to each other before the cell is glued together (as in Fig. 1). The alignment is done by hand. The glass plates are separated by spacers of 3µm. To achieve electrical tuning, a sinusoidal potential difference with a frequency of 1kHz is applied over the ITO electrodes.

To analyze the diffraction, a continuous wave He-Ne laser (JSD uniphase, 633nm, 4mW) is used and the diffraction efficiency is detected with a power meter (Newport 2936C). The He-Ne light source is linearly polarized and the polarization state is controlled by a quarter waveplate (QWP). Microscope pictures are taken with a polarizing optical microscope (Nikon Eclipse E400 POL).

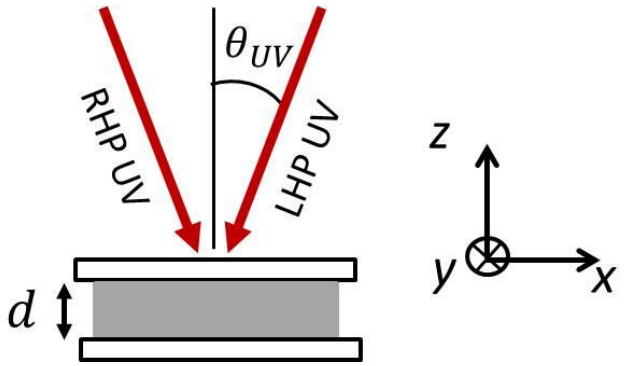

Figure 2 illumination scheme for a 1D LC polarization grating (RHP and LHP UV = right- and left-handed circularly polarized UV light).

Polarization microscopy analysis

Polarizing optical microscopy can help to reveal the director configuration in the bulk of the LC cell. Figure 3 shows transmission microscope images for a cell between crossed polarizers without voltage applied. The boundary conditions determined by photo-alignment are periodic with a unit cell with dimensions Λ by Λ. However, the unit cell of the liquid crystal 2D structure has an area of $4*\Lambda^2$ and two domains with shifted gratings may be observed (figure 3 and 4). The fact that the liquid crystal forms a superstructure with a lower periodicity than the structure defined by the boundary conditions, is reminiscent of a symmetry breaking that takes place in order to avoid the formation of disclinations and to reduce the total free energy in the director configuration. Figure 3 illustrates the existence of two domains in which the pattern in shifted horizontally over a distance Λ. Symmetry breaking leads to equivalent structures with different properties that can be used in bistable devices that can be switched electrically or optically[24].

The complex pattern contains a purple line with little variation in intensity along the diagonal. When the amplitude of the ac voltage is increased the smooth color pattern changes continuously until a dark state is obtained, indicating that the equilibrium structure does not contain any disclination lines (figure 5). With the director orientation at the two substrates determined by photo-alignment, it is not possible to achieve a continuous (disclination-free) director distribution in which all directors lie in the horizontal *xy*-plane. As we do not observe disclinations, we can conclude that the director configuration will have components along the z-direction.

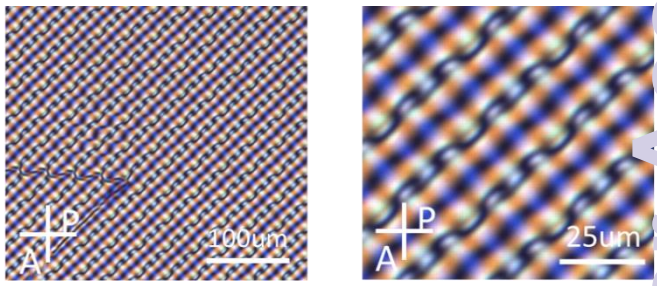

Figure 3 transmission profile of the LC cell between crossed polarizers (0V)

As can be seen in figure 4, the period along the anti-diagonal is $\sqrt{2}*\Lambda$ and not $\Lambda/\sqrt{2}$. Along the solid black lines on figure 4 the top and bottom director are parallel, while on the dashed black lines the top and bottom director are antiparallel. Although there is no physical difference between ***n*** and ***-n***, the symmetry breaking that takes place in order to avoid the formation of disclinations makes these two configuration in the superstructure nonequivalent.

Based on the transmission microscope images, we can estimate a director configuration in the bulk of the LC cell. Figure 4 shows the proposed mid-plane director orientation on the right. This configuration is consistent with the experimentally observed absence of disclination lines and can explain the $\sqrt{2}*\Lambda$ periodicity along the anti-diagonal. For

positions with a parallel top and bottom director (solid lines) the director configuration in the bulk is approximately homogeneous. This yields a retardation of $\Gamma \approx (2\pi\Delta n\, d)/\lambda \approx (2\pi * 0.22 * 3)/\lambda[\mu m]$ close to 2π for red light which explains the dark blue diagonal in the picture. For the dotted lines in the figure with an antiparallel top and bottom plane director the mid-plane director is vertical. This gives rise to a retardation close to π for red and green light and a bright area if the director is not parallel to the polarizer or analyzer.

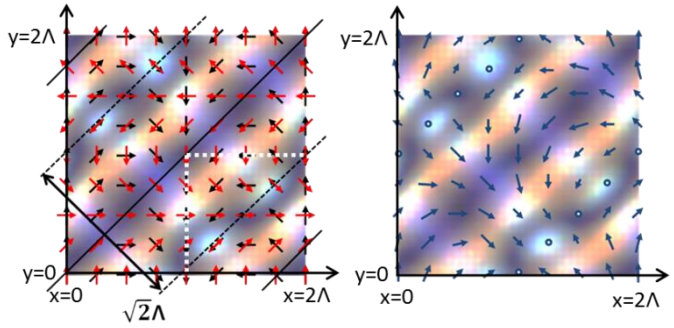

Figure 4 transmission profile with top (red) and bottom (black) director distribution (left); transmission profile with mid-plane (blue) director distribution (right). One unit cell for the director configuration is shown in the figures, the unit cell for the boundary conditions is shown in a dotted line.

The observed transmission between crossed polarizers for three different voltages is shown in figure 5. For sufficiently high voltages (≥3Vp), the structure becomes centro-symmetric with a periodic pattern along both the diagonal and the anti-diagonal. The periodicity in this case is $\Lambda/\sqrt{2}$ in both directions. For high voltages we expect the director to be along the z-axis in the middle of the LC, whereas there is still planar alignment near the substrates. If the directors at the top and bottom substrates are oriented perpendicularly, the transmission is low and a dark spot is visible (figure 6). This can be explained by the fact that the retardation of the LC layers near the top and near the bottom substrates have opposite sign and compensate each other. Positions with a parallel director orientation at top and bottom substrates also give rise to dark areas if the orientation is also parallel with the polarizer or the analyzer. For high voltages, the transmission becomes very low since the LC is then almost completely vertically aligned and the retardation is close to zero.

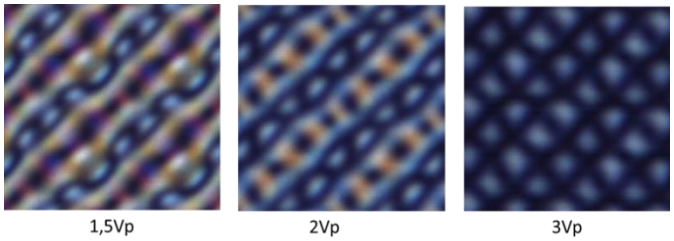

Figure 5 transmission profile between crossed polarizers for 1.5Vp, 2Vp and 3Vp.

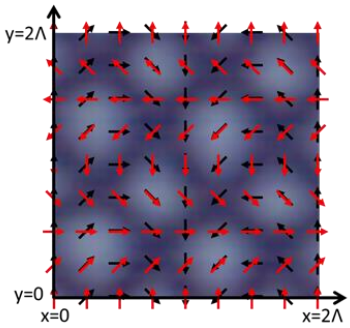

Figure 6 transmission profile between crossed polarizers for 4Vp.

FE simulations

Theory

The spatial distribution of the nematic director in a volume is found by minimizing the Landau-de Gennes free-energy functional[25-26]. The liquid crystal is described by an ord tensor (Q-tensor) and the given alignment conditions at the top and bottom interfaces are included using strong anchori conditions. The unit cell considered in the simulations has dimension 2Λ in both the *x*- and *y*-direction so the simulated 3D domain has a volume of 2Λ*2Λ*d with *d* the thickness of the cell. The Landau-de Gennes total free energy in the LC domain Ω, in contact with a surface Γ is

$$f_{total} = \int_{\Omega}(f_B + f_D - f_E)\, d\Omega + \int_{\Gamma} f_S\, d\Gamma$$

where f_B is the thermotropic bulk energy density, f_D is the elastic distortion energy density, f_E is the electrostatic energy density and f_S is the surface energy density.

Since strong anchoring is assumed, the surface anchoring term can be neglected and the LC orientation is fixed at the boundary. The pretilt is set equal to zero and the azimuth angle varies as $\varphi(x) = \left(\frac{\Lambda}{2} - x\right) * \frac{\pi}{\Lambda}$ on the bottom substrate and $\varphi(y) = \left(\frac{\Lambda}{2} - y\right) * \frac{\pi}{\Lambda}$ on the top substrate.

The thermotropic energy density is given by

$$f_B = \frac{A}{2}tr(Q^2) + \frac{B}{3}tr(Q^3) + \frac{C}{4}tr(Q^2)^2$$

in which we use $A = -2 * 0.87 * 10^3\, N/m^2$, $B = -2.12 * 10^4\, N/m^2$ and $C = 1.74 * 10^4\, N/m^2$ for the bulk thermotropic coefficients. These values of *A*, *B* and *C* are two orders of magnitude smaller than the experimentally measured values for 5CB[27]. Using 100 times lower values for these constants increases the natural length scale of variation in the order parameter and results in a faster numerical convergence of the problem, as reported previously in the literature[28-30]. As we do not expect large order parameter variations, due to the fact that no disclinations are present, this is a good approximation.

The distortion energy and electrostatic energy density contributions are respectively:

$$f_D = \frac{1}{2}L_1 Q_{\alpha\beta,\gamma}Q_{\alpha\beta,\gamma} + \frac{1}{2}L_2 Q_{\alpha\beta,\beta}Q_{\alpha\gamma,\gamma} + \frac{1}{2}L_6 Q_{\alpha\beta}Q_{\mu\nu,\alpha}Q_{\mu\nu,\beta}$$

$$f_E = \frac{1}{2}\epsilon_0(E_\alpha \epsilon_{\alpha\beta} E_\beta)$$

where L_1, L_2 and L_6 are constants that can be related to the splay, twist and bend elastic constants K_{11}, K_{22} and K_{33}, $\epsilon_{\alpha\beta}$ is the permittivity tensor and **E** is the electric field. The algorithm seeks for the Q-tensor field that renders the energy functional stationary and the electrostatic field is determined from the variational form of Laplace's equation[31]. The elastic and dielectric properties of the liquid crystal E7 are used in the simulation (K_{11}=11.1pN, K_{22}=6.5pN, K_{33}=17.1pN, $\epsilon_\perp$=5.2 and $\epsilon_{//}$=19.0).

Direct minimization of the Landau-de Gennes energy, without a reasonably close initial guess for the Q-tensor is computationally intensive. Based on the experimentally observed microscope pictures and the conclusions drawn in section 3 we could make a good initial guess for the director profile.

For the 3D FE simulation of the Q-tensor model, a tetrahedral volume mesh is used. To calculate the optical transmission through the structure, the result for the Q-tensor is interpolated on a regular grid. This makes it possible to use the Jones matrix formalism for the transmission after calculating of the azimuth and inclination from the Q-tensor. In order to obtain a rough comparison with the microscopy images, we combine the simulated transmission patterns for blue (λ=450nm), green (λ=550nm) and red (λ=650nm) light into a color image.

Simulations

The director configuration is strongly influenced by the ratio between the periodicity Λ and the thickness d of the cell. For thin cells with a large Λ/d ratio, a structure with planar directors will be favored while for thick cells with a small Λ/d ratio the director configuration will be close to vertical in the bulk. When the Λ/d ratio is decreasing, we expect the cell configuration to change from mainly planar directors with twist disclination lines to a mixed configuration with both horizontally and vertically aligned regions in the middle as shown in figure 4 and 7. The tilt in the quasi-planar regions keeps increasing for decreasing Λ/d ratios until the director orientation is almost completely vertical in the bulk (figure 8 and 9). Applying a voltage to the cell, also makes vertical director orientation in the bulk of the cell more favorable (figure 7-9).

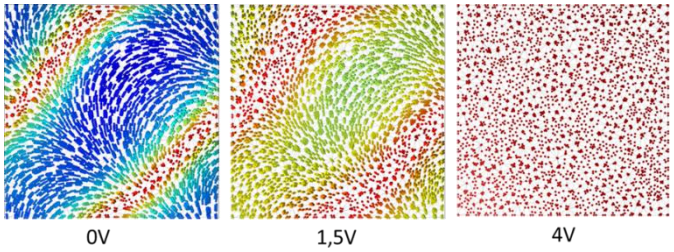

Figure 7 simulated mid-plane (z=1.5µm) director profile for 0V, 1.5V and 4V for a cell with 2Λ*2Λ*d=13µm*13µm*3µm.

The investigated cells have a Λ/d ratio equal to $6.5\mu m/3\mu m$ and the equilibrium configuration agrees with the intermediate state with both vertical and quasi horizontal regions in the middle (figure 7-9). The simulated director configuration agrees well with the one theoretically predicted based on the microscope images (figure 4). The simulations show that the minimal tilt in the middle of the cell is not equal to 0° but around 8°. When a voltage is applied to the cell, the degree of vertical alignment in the bulk increases as can be seen in figures 7 to 9. The simulations confirm the director configuration presented in the previous section.

For the cases with and without applied voltage, the simulated transmission profiles (figure 10) are in good agreement with the experimentally observed profiles (figure 4 and 5). The periodicity, the bright and dark areas and even the color information is reproduced to a good degree. This confirms the validity of the solution for the director configuration.

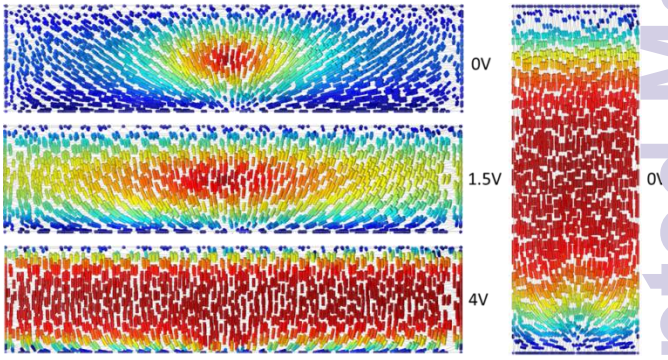

Figure 8 simulated director profile for a cell with 2Λ*2Λ*d=13µm*13µm*3µm (left) and 2Λ*2Λ*d=3.25µm*3.25µm*9µm (right). The applied voltage is 0V on the right and 0V, 1.5V and 4V on the left from top to bottom. A cross section of the director profile for y=0 is shown.

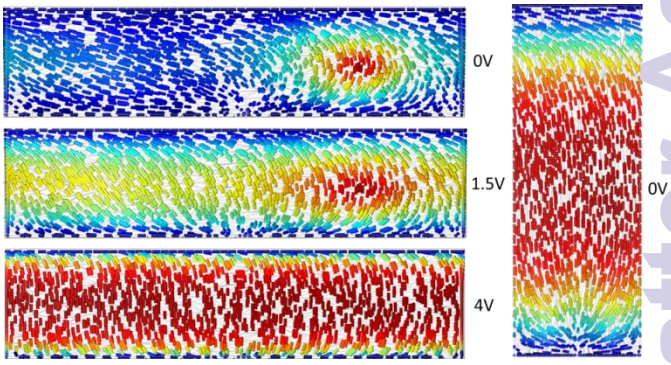

Figure 9 simulated director profile for a cell with 2Λ*2Λ*d=13µm*13µm*3µm (left) and 2Λ*2Λ*d=3.25µm*3.25µm*9µm (right). The applied voltage is 0V on the right and 0V, 1.5V and 4V on the left from top to bottom. A cross section of the director profile for y=Λ/2 is shown.

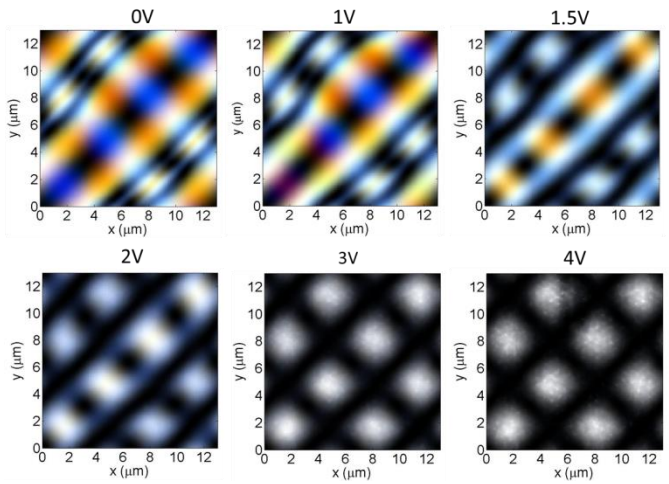

Figure 10 simulated transmission patterns for a cell with 2Λ*2Λ*d=13μm*13μm*3μm. The applied voltages are 0V, 1V, 1.5V, 2V, 3V and 4V.

Diffraction Patterns

Theory and simulation

For 1D LC polarization gratings the diffraction efficiency of the different modes can be estimated theoretically[13,16] based on the paraxial approximation for an infinite grating with $2\pi\lambda d/(n_0\,\Lambda^2) < 1$. The theoretical prediction for the diffraction efficiency η_m of the mth-order is

$$\eta_0 = cos^2\left(\frac{\pi\Delta nd}{\lambda}\right)$$

$$\eta_{\pm 1} = \frac{1}{2} * [1 \mp S_3']sin^2\left(\frac{\pi\Delta nd}{\lambda}\right) \qquad (1)$$

$$\eta_m = 0 \text{ for all } m \geq 2$$

with λ the wavelength of the incident light and $S_3' = S_3/S_0$ the normalized Stokes parameter corresponding to the ellipticity of the incident light[16]. The polarization state is conserved for diffraction in the 0th order and the handedness of circular polarization is inversed for diffraction in the 1th order. Δn can be approximately simulated as a function of the voltage by considering the electrostatic switching of a planar nematic LC cell. For the diffraction grating studied in this article, it is no longer possible to calculate the diffraction efficiency theoretically. For sufficiently high voltages (>1V), we are however able to use the results for a one dimensional LC polarization grating. Besides other elements, for these voltages the diffraction pattern contains two diffraction spots originating from the one-dimensional gratings in the *x*- and *y*-directions. The director in the upper part of the cell stays unchanged for a constant *y*-coordinate while the director in the lower part of the cell stays unchanged for a constant *x*-coordinate. For this reason the cell acts as a combination of a diffraction grating along the *x*-direction and one along the *y*-direction. The behavior of these 1D gratings as a function of the voltage can be estimated theoretically based on equation (1). The combined effect of the upper and lower part of the cell gives rise to an overall periodicity along the anti-diagonal and a diffraction spot in this direction (figure 11).

A more elaborate theoretical study of the 2D diffraction grating for lower voltages is not considered in this article. Instead the diffraction pattern is numerically calculated based on the simulated director profile. By performing the Jones calculus as described in the previous section, the phase and polarization state of the wave is known after propagating through the liquid crystal layer. To calculate the diffraction pattern, the wave is decomposed into two waves with orthogonal linear polarizations (along the *x*- and *y*-axis) and the diffraction is found by using a 2D Fourier transform for both near field components. Both the polarization state and the diffraction intensity in the different orders can be found by combining the two diffraction patterns.

Experiments

In the diffraction experiment, right handed circularly polarized light from a He-Ne laser (633nm) is used. For left handed circularly polarized light, the same results are obtained with the diffraction spots mirrored through the origin. The incident power is 200μW. The total transmission in the measured diffraction orders depends on the applied voltage but is typically around 80%. This means that around 20% of the light is scattered, absorbed or reflected by the LC cell.

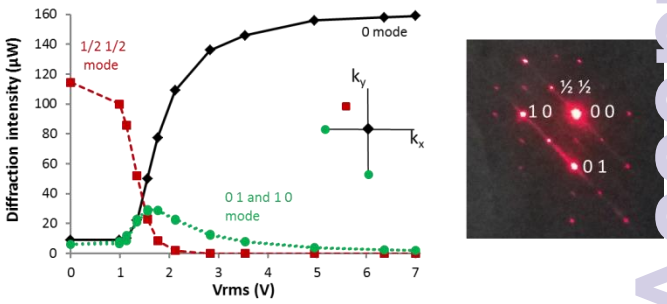

Figure 11 left: measured diffraction intensity as a function of the voltage for the ½ ½ mode, 0 1 mode, 1 0 mode and 0 mode. Right: the pattern appearing on a screen, seen from the laser, for an applied voltage of 2V.

When no voltage is applied, only a few percent of the light is transmitted in the zero order, and almost 60% of the incident light is diffracted into the ½ ½ order (figure 11). Despite the complicated director configuration, the diffraction efficiency is still relatively high thanks to the high quality of the structure. Since the director pattern shows a $\sqrt{2}*\Lambda$ periodicity along the anti-diagonal the light is most strongly diffracted in the ½ ½ order situated along the anti-diagonal (figure 11). By increasing the voltage, the diffraction into the ½ ½ order decreases while the transmission in the zero order increases. Above the threshold voltage (≈0.9V), both the director configuration and the diffraction pattern start to change abruptly. For high voltages (>3V) the director configuration slowly becomes vertical in the bulk and the diffraction in the zero order converges to the maximum. The threshold voltage is on the same order of magnitude as the theoretically calculated and

experimentally observed threshold voltage for 1D LC polarization gratings[18].

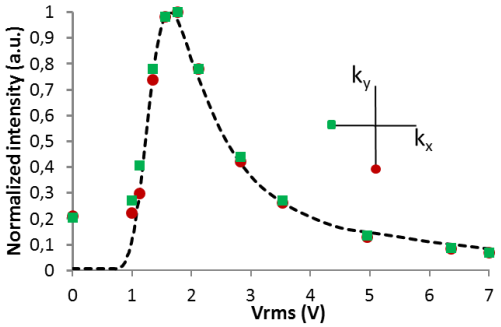

figure 12 theoretical prediction for the diffraction into the first order (black) and experimentally measured diffraction in the 0 1 and 1 0 orders (red and green) as a function of the voltage.

Besides diffraction in the ½ ½ and zero order modes, a considerable amount of light is diffracted in the 0 1 and 1 0 modes for intermediate voltages (0.9V<V<3V). This diffraction is similar to the one observed for 1D LC polarization gratings with the same periodic alignment layer on both substrates (only in the *x*- or only in the *y*-direction). For high voltages, the problem is actually decoupled into two problems where the top and bottom alignment layer act independently. As explained earlier, at high voltages the director in the upper part of the cell stays unchanged for a constant *y*-coordinate while the director in the lower part of the cell stays unchanged for a constant *x*-coordinate.

The combined effect of the upper and lower part gives rise to an overall periodicity along the anti-diagonal and causes the ½ ½ diffraction spot. The periodicity along the *x*-direction and *y*-direction is equal to Λ while the periodicity along the anti-diagonal is $\sqrt{2}*\Lambda$, which agrees with the relative position of the 1 0, 0 1 and ½ ½ diffraction spots. In figure 12, the diffraction intensity in spots 1 0 and 0 1 as a function of the voltage is compared to the theoretical prediction for a cell of 2.8µm thickness (equation 1). The results are normalized such that the behavior as a function of the voltage can be easily compared. A good agreement between theory and the experiment is observed.

Since only the behavior of the 1 0 and 0 1 diffraction modes can be compared with the theory, we performed a fast Fourier transform to simulate the complete diffraction pattern based on the results from the Jones calculus. This analysis was repeated for different voltages and the results are compared with the experiment in figures 13 and 14. The diffraction in the ½ ½ and 0 0 mode is analyzed in figure 13 while the 0 1, 1 0 and some less strong diffraction orders are given in figure 14. The experimental results are shown in red while the simulations are shown in black. In general, a good agreement between the experiments and the simulations is observed. The alignment is not perfect in practice and the diffraction pattern depends strongly on the thickness of the cell. Small changes between the simulations and the experiment can be related to this.

Our simulations show that the polarization state is conserved for the 0th order diffraction and changed from right- to left-handed polarization for the 0 1 and 1 0 diffraction orders at high voltages. This confirms that the 2D grating at high voltage can be considered as a combination of two 1D gratings[16].

When the incident laser beam makes a (small) angle with the substrate normal, the diffraction patterns are similar to the results presented previously. This is not unexpected, because the cell thickness is much smaller than the grating period.

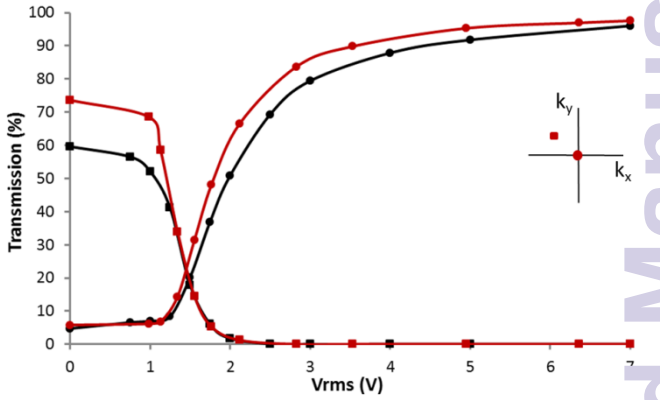

figure 13 experimental measurements (red) and simulations (black) for the diffraction in the 0 mode and ½ ½ mode.

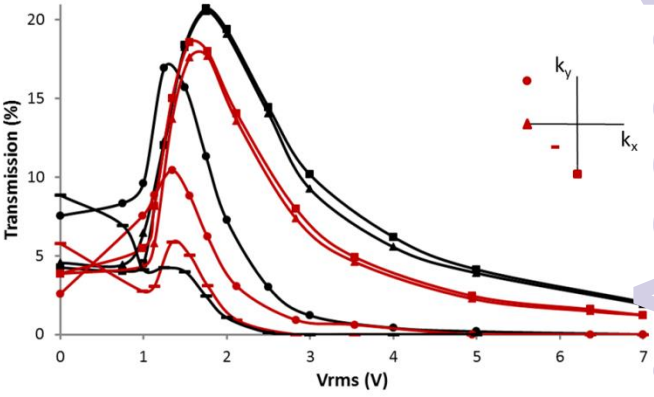

Figure 14 experimental measurements (red- and simulations (black) for the diffraction in the 1 0, 0 1, 1 1 and -½ ½ mode.

Conclusions

We have demonstrated that it is possible to form a periodic two-dimensional liquid crystal grating by separately illuminating the photo-alignment layers on two substrates with one-dimensional UV interference patterns. Remarkably, the liquid crystal director pattern that is formed between the alignment layers has a lower periodicity (the period is two times larger) than the interference pattern of the alignment layers. The resulting liquid crystal lattice has a topology without disclinations and is rather complicated. By careful analysis of microscopy images and diffraction patterns and by comparing them with numerical simulation results, we a

confident that we have a good knowledge of the resulting 3D director distribution.

In order to demonstrate the validity of the director orientation we used a period of 6.5μm for the interference pattern. Smaller periods, leading to larger diffraction angles can equally be used. By increasing the angle θ_{UV} of the UV laser beams, the period of the grating Λ can be reduced and the resulting angles of diffraction can be increased considerably. To obtain the same complex 3D director pattern, the cell thickness d should be scaled down linearly with the period Λ, however this will reduce the fraction of light that is diffracted in the non-zero order. Decreasing the Λ/d ratio on the other hand will lead to a weak diffraction grating with a close to vertical director orientation in the bulk.

This work demonstrates that a complex, 3D liquid crystal pattern can be formed in the bulk by defining a well-designed director orientation on two planar substrates. We have presented only one possibility, but photo-alignment patterns may prove to be a versatile procedure to realize a myriad of 3D liquid crystal structures. The fact that symmetry breaking leads to structures with a larger period indicates that the boundary conditions may lead to inherently equivalent stable states that could be selected by the application of small inhomogeneous electric fields. This opens up promising applications for ultra-low power devices. The presented work offers interesting perspectives for beam-steering devices and laser applications.

Acknowledgements

The authors would like to acknowledge funding by the Flemish Fund for Scientific Research (FWO), the IAP project photonics@be and the IWT project SECONDOS. Dr. Yi Xie and the students Blommaert Andreas, Meeus Laurens and Tarnaud Thomas are acknowledged for their exploring technological work and V. G. Chigrinov and Beamco are acknowledged for providing the photo-alignment materials.

Notes and references

1 C.-C. Chen, W.-F. Chiang, M.-C. Tsai, S.-A. Jiang, T.-H. Chang, S.-H. Wang, C.-Y. Huang, Optics Letters, 2015, **40**, 2021.
2 P.-C. Chien, T.-K. Lin, S.-A. Jiang, J.-H. Liu, H.-Y. Miao, Y.-W. Chen, C.-Y. Huang, Optical Materials Express, 2015, **5**, 1399.
3 D. Xu, G. Tan, S.-T. Wu, Optics Express, 2015, 23, 12274.
4 D. C. Zografopoulos, R. Beccherelli, E. E. Kriezis, Physical Review E, 2014, **90**, 042503.
5 U. Ruiz, P. Pagliusi, C. Provenzano, E. Lepera, G. Cipparrone, Applied Optics, 2015, **54**, 3303.
6 J. Sun, S.-T. Wu, and Y. Haseba, Applied Physics Letters, 2014, **104**, 023305.
7 H. Coles, and S. Morris, Nature Photonics, 2010, **4**, 676.
8 J. Beeckman, K. Neyts and P. J. M. Vanbrabant, Optical Engineering, 2011, **50**, 081202.
9 C. X. Zhao, F. Fan, T. Du, V. G. Chigrinov, and H. S. Kwok, *Optics Letters*, 2015, **40**, 2993.
10 V. G. Chigrinov, A. Muravski and H. S. Kwok, *Physical Review E*, 2003, **68**, 061702.
11 V. G. Chigrinov, *Crystals*, 2003, **3**, 149.
12 E. A. Shteyner, A. K. Srivastava, V. G. Chigrinov, H.-S. Dwok and A. D. Afanasyev, Soft Matter, 2013, **9**, 5160.
13 J. Tervo and J. Turunen, Optics Letters, 2000, **25**, 785.
14 J. N. Eakin, Y. Xie, R. A. Pelcovits, M. D. Radcliffe and G. P. Crawford, Applied Physics Letters, 2004, **85**, 1671.
15 V. Presnyakov, K. Asatryan, T. Galstian and V. G. Chigrinov, Optics Express, 2006, **14**, 10558.
16 M. J. Escuti and W. M. Jones, SID Symposium Digest., 2006, **37**, 1443.
17 R. K. Komanduri, W. M. Jones, C. Oh and M. J. Escuti, Journal of the Society for Information Display, 2007, **15**, 589.
18 R. K. Komanduri and M. J. Escuti, Physical Review E, 2007, **76**, 021701.
19 R. K. Komanduri, C. Oh and M. J. Escuti, Proc. Of SPIE, 2008, **7050**, 70500J-1.
20 E. A. Shteyner, A. K. Srivastava, V. G. Chigrinov, H.-S. Dwok and A. D. Afanasyev, Soft Matter, 2013, **9**, 5160.
21 T. Sasaki, H. Ono, and N. Kawatsuki, Applied Optics, 2008, **47**, 2192.
22 H. Choi, and J. W. Wu, Journal of the Optical Society of America B, 2009, **26**, 1.
23 V. Chigrinov, E. Prudnikova, V. Kozenkov, Z. Ling, H. S. Kwok, H. Akiyama, T. Kawara, H. Takada and H. Takatsu, SID Symposium Digest of Technical Papers, 2002, **33**, 1106.
24 I. I. Smalyukh, Y. Lansac, N. A. Clark and R. P. Trivedi, Nature Materials, 2010, **9**, 139.
25 P. G. de Gennes and J. Prost, *The Physics of Liquid Crystals*, Clarendon Press, Oxford, 2nd edn., 1993, ch. 2, pp. 76-78.
26 L. D. Landau, E. M. Lifshitz and L. P. Pitaevskii, *Statistical Physics*, Pergamon Press, Oxford, 3rd edn., vol. 5., 1980, ch 8, pp. 440-442.
27 H. J. Coles, Molecular Crystals and Liquid Crystals, 1978, **49**, 67.
28 L. A. Parry-Jones and S. J. Elston, Journal of Applied Physics, 2005, **97**, 093515.
29 E. Willman, F. A. Fernández, R. James and S. E. Day, Journal of Display Technology, 2008, **4**, 276.
30 A. J. Davidson, C. V. Brown, N. J. Mottram, S. Ladak and C. R. Evans, Physical Review E, 2010, **81**, 051712.
31 R. James, E. Willman, F. A. Fernández and S. E. Day, IEEE Transactions on Electron Devices, 2006, **53**, 1575.